

pubs.acs.org/JACS Communication

# Coordination-Induced Weakening of a C(sp³)-H Bond: Homolytic and Heterolytic Bond Strength of a CH-Ni Agostic Interaction

Lirong Lin, Denis M. Spasyuk, Roger A. Lalancette, and Demyan E. Prokopchuk\*



Cite This: J. Am. Chem. Soc. 2022, 144, 12632–12637



**ACCESS** 

Metrics & More

Article Recommendations

s Supporting Information

**ABSTRACT:** The scission of a  $C(sp^3)$ -H bond to form a new metal-alkyl bond is a fundamental step in coordination chemistry and catalysis. However, the extent of C-H bond weakening when this moiety interacts with a transition metal is poorly understood and quantifying this phenomenon could provide insights into designing more efficient C-H functionalization catalysts. We present a nickel complex with a robust adamantyl reporter ligand that enables the measurement of C-H acidity  $(pK_a)$  and bond dissociation free energy (BDFE) for a  $C(sp^3)$ -H agostic interaction, showing a decrease in  $pK_a$  by dozens of orders of magnitude and BDFE decrease of about 30 kcal/mol upon coordination. X-ray crystallographic data is provided for all molecules, including a distorted square planar Ni<sup>III</sup> metalloradical and "doubly agostic" Ni<sup>II</sup>  $(\kappa^2$ -CH<sub>2</sub>) complex.

he transition metal catalyzed functionalization of unactivated  $C(sp^3)$ -H bonds has emerged as a powerful tool to synthesize chemicals of importance to the pharmaceutical and agrochemical industries. Ni- and Pd-catalyzed C(sp<sup>3</sup>)-H functionalization typically involves a rate-limiting C(sp<sup>3</sup>)-H activation step, where the chelating ligands direct the C-H bond near the metal center before generating the M-C covalent bond. It is generally accepted that this crucial step proceeds through a transient intermediate containing a C-H—M agostic interaction (i.e., 3-center-2-electron M-H-C bond)<sup>2</sup> that reacts with internal or exogenous base through a concerted-metalation deprotonation (CMD) pathway (Figure 1, left). However, since one-pot synthetic protocols assemble the active species in situ, it is difficult to quantify the magnitude of C-H bond weakening prior to M-C bond formation in this elementary step. Therefore, obtaining thermochemical data through acidity  $(pK_a)$  and bond dissociation free energy (BDFE) measurements on sterically

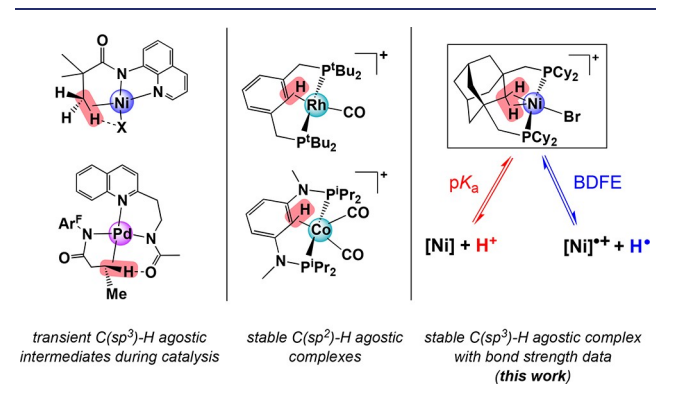


**Figure 1.** Formation of transient agostic intermediates via substrate directing groups (left); Rh and Co complexes containing agostic  $C(sp^2)$ -H interactions (middle); the  $C(sp^3)$ -H agostic Ni complex used in this study (right).

and electronically tunable model systems might provide insights into designing more efficient  $C(sp^3)$ —H functionalization catalysts.

In a related context,  $C(sp^2)-H-M$  agostic interactions have been studied in detail. The C-H acidity of coordinated  $Pd^{II}(\eta^2\text{-arene})$  interactions were recently estimated to have  $pK_a^{\text{MeCN}}$  values between 3 and 6. Structurally authenticated  $C(sp^2)-H$  agostic pincer complexes resembling Wheland-type intermediates have also been studied (Figure 1, middle). A  $[Rh(P(\eta^2\text{-}C_{aryl}H)P)]^+$  complex can be deprotonated to yield a square planar Rh(PCP) pincer complex, while the reaction of a  $Co(P(C_{aryl})P)$  complex with acid generates  $[Co(P(\eta^2\text{-}C_{aryl}H)P)]^+$ . Bond strength measurements were not reported in these examples; however, they demonstrate the potential for using pincer-type motifs as blueprints to study the thermochemistry of agostic C-H interactions.

To study analogous  $C(sp^3)$ –H—M interactions, the choice of  $PC(sp^3)P$  ligand framework is critical because rapid  $\alpha$ -H or  $\beta$ -H elimination reactions can occur, resulting in carbene and olefin products. We rationalized that kinetically stable molecules could be obtained by using a rigid and sterically bulky adamantane ligand skeleton that is also immune to  $\beta$ -H elimination (Figure 1, right). Gratifyingly, this robust adamantyl ligand framework stabilizes a  $Ni^{II}$ – $(C(sp^3)$ –H) agostic interaction, providing an unprecedented opportunity to study the thermochemical driving forces behind nickel-mediated C–H bond scission.

The known 1,3-bis(dicyclohexylmethylphosphino)-adamantane ligand  $PCH_2P^{9,10}$  is combined with  $NiBr_2(PPh_3)$ ,

Received: May 31, 2022 Published: July 5, 2022





to generate pale yellow [Ni-CH] in low yield and is purified by column chromatography under air (Scheme 1). Several

# Scheme 1. Synthesis and Reactivity of [Ni-CH]

bases were screened, however none improve the yield. Mass spectrometry and UV–vis spectroscopy indicate that the major product is [HPCH<sub>2</sub>P][NiBr<sub>3</sub>] (see SI). Important NMR spectral features for [Ni–CH] include peaks at 1.81 ppm ( $^{1}\text{H}$ ) and 64.6 ppm ( $^{13}\text{C}$ ) for the Ni–CH<sub>alkyl</sub> moiety, while a  $^{31}\text{P}$  singlet appears at 49.0 ppm. The Ni–C bond distance is 1.987(4) Å (Figure 2), which is typical in relation to other NiBr pincer complexes.  $^{12}$ 

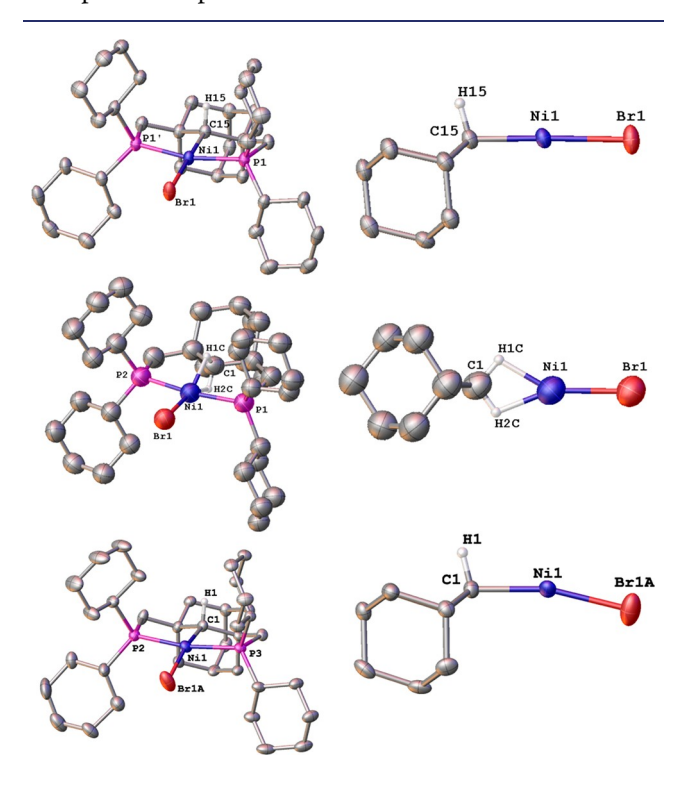


**Figure 2.** Molecular structures (50% probability ellipsoids) of [Ni–CH] (top), [Ni–CH<sub>2</sub>]<sup>+</sup> (middle), and [Ni–CH]<sup>\*+</sup> (bottom) with core structures shown on the right. Most H atoms, cocrystallized solvent, and  $B(C_6F_5)_4^-$  are omitted for clarity. Key metrical parameters are provided in the Supporting Information.

Protonation of [Ni-CH] with Jutzi's acid [H(OEt<sub>2</sub>)<sub>2</sub>][B- $(C_6F_5)_4]^{13}$  in PhF at -40 °C changes the solution color from pale yellow to deep purple, with new UV-vis spectral maxima at 360 ( $\varepsilon$  = 5700 M<sup>-1</sup> cm<sup>-1</sup>) and 559 nm ( $\varepsilon$  = 1760 M<sup>-1</sup> cm<sup>-1</sup>; Figures S14 and S15). The air-sensitive purple solid is unstable in donor solvents, such as THF and MeCN. <sup>1</sup>H NMR spectroscopy in  $CD_2Cl_2$  reveals a broad triplet at -1.36 ppm that integrates for two protons relative to all other alkyl resonances. Structural elucidation reveals the agostic complex  $[NiBr(P(\kappa^2-CH_2)P)][B(C_6F_5)_4]$  ( $[Ni-CH_2]^+$ ), featuring a methylene group that is symmetrically interacting with Ni through both  $C(sp^3)$ -H moieties of adamantane, akin to the behavior of bidentate  $\kappa^2$ -[BH<sub>4</sub>]<sup>-</sup> ligands (Figure 2, middle).<sup>14</sup> This "doubly agostic"  $\kappa^2$ -CH<sub>2</sub> bonding motif<sup>15</sup> represents the first example of a  $\kappa^2$ -CH<sub>2</sub> group interacting with a Ni<sup>II</sup> center (Figure 2). A similar type of symmetric bis(C-H) agostic interaction has been structurally determined at a Ni<sup>I</sup> center<sup>16</sup> and recent electronic structure studies reveal direct Ni-C bonding.<sup>17</sup> Reaction with 2,4,6-trimethylpyridine in PhF cleanly regenerates [Ni-CH] as the sole product by <sup>31</sup>P NMR.

When compared to the canted adamantyl skeleton of [Ni-CH], the  $\kappa^2$ -CH<sub>2</sub> ligand of adamantane is symmetrically oriented along the  $(\kappa^2$ -CH<sub>2</sub>)-Ni-Br bonding axis (Figure 2, right). Hydrogen atoms H1C and H2C are freely refined, resulting in very similar Ni-H bond lengths (1.69(5) and 1.66(6) Å) and C1-H-Ni angles (100.1 and 103.9°). Although the acute C-H-Ni angles are within range to be considered agostic (~90-140°), the Ni-H bond lengths fall within the lower extreme of the  $\sim$ 1.8–2.3 Å range commonly ascribed to such interactions.<sup>2</sup> Because of the weakened transinfluence of the  $\kappa^2$ -CH<sub>2</sub> moiety of [Ni-CH<sub>2</sub>]<sup>+</sup>, the Ni-Br bond contracts by 0.18 Å relative to [Ni-CH]. Furthermore, computational (DFT) geometries are in good agreement with the X-ray structural data for all nickel complexes presented in this study (Table S2). Geometry optimizations were performed at the TPSS-D3(BJ)/def2-TZVP level of theory, <sup>18</sup> which is particularly effective at modeling agostic interac-

NMR spectroscopic characterization in CD<sub>2</sub>Cl<sub>2</sub> indicates that [Ni-CH<sub>2</sub>]<sup>+</sup> retains the same structure in the solution phase. By <sup>1</sup>H NMR, the shielded triplet at -1.36 ppm has a small  ${}^{1}H-{}^{31}P$  coupling constant ( ${}^{2}J_{HP}=5.5$  Hz) that collapses to a singlet with <sup>31</sup>P decoupling (Figure S8). Additionally,  $^{13}C\{^{1}H\}$  NMR data reveals a triplet at 48.5 ppm ( $^{3}J_{CP} = 17$ Hz) belonging to the  $\kappa^2$ -CH<sub>2</sub> moiety, as confirmed by  $^1$ H $^{-13}$ C HSQC (Figure S9). The decreased <sup>1</sup>J<sub>HC</sub> coupling constant of the *ipso*-carbon by proton-coupled  $^{13}$ C NMR ( $^{1}J_{HC} = 106$  Hz) also verifies the agostic nature of this bonding interaction, since  ${}^{1}J_{HC}$  = 124 Hz for a nonagostic methylene group within the PCH<sub>2</sub>P ligand skeleton (Figure S6). To explore the possibility of a solution-phase equilibrium between [Ni-CH<sub>2</sub>]<sup>+</sup> and a Ni<sup>IV</sup>H C-H oxidative cleavage product, DFT calculations were performed. Multiple attempts to optimize a Ni<sup>IV</sup>H adduct resulted in convergence to the doubly agostic [Ni-CH<sub>2</sub>]<sup>+</sup>. Therefore, the spectroscopic, computational, and solid-state metrical parameters collectively indicate that Ni- $(\kappa^2$ -CH<sub>2</sub>) bonding is agostic in the solid state and in solution under ambient conditions.

Cyclic voltammograms (CVs) of [Ni–CH] with 0.1 M ["Bu<sub>4</sub>N][B( $C_6F_5$ )<sub>4</sub>] in THF under N<sub>2</sub> show a diffusion-controlled Ni<sup>III/II</sup> redox couple ( $E_{1/2} = +0.155$  V). Similar redox behavior is also observed when using the weakly coordinating solvent 1,2-dichloroethane (DCE;  $E_{1/2} = +0.110$ 

V) (Figure S18).<sup>20</sup> Preparation of the 15e<sup>-</sup> metalloradical cation  $[Ni-CH][B(C_6F_5)_4]$  was achieved by dropwise addition of pale yellow [Ni-CH] to a stirring suspension of the "magic blue" aminium salt  $[(p-C_6H_4Br)_3N][B(C_6F_5)_4]^{21}$  in toluene at -78 °C (Scheme 1). Deep orange-red [Ni-CH]\*+ has UV-vis spectral maxima at 357 ( $\varepsilon$  = 2420 M<sup>-1</sup>cm<sup>-1</sup>) and 404 nm ( $\varepsilon = 2110 \text{ M}^{-1}\text{cm}^{-1}$ ; Figure S17). A spin-only magnetic moment of 1.78  $\mu_B$  is consistent with an S = 1/2ground state (C<sub>6</sub>D<sub>5</sub>Br, Evans method). X-ray quality single crystals were grown via toluene/pentane vapor diffusion at room temperature, confirming the molecular structure of Ni-CH] •+ (Figure 2, bottom). The Br ligand is positionally disordered over two sites in the crystal lattice in a 0.71:0.29 ratio with the major component adopting a distorted square planar geometry  $(\tau_4 = 0.18)^{22}$  with a C-Ni-Br angle of 165.96(11)° and Ni-Br1A distance of 2.2677(8) Å. The minor component is less distorted ( $\tau_4 = 0.15$ ) because of a more obtuse C-Ni-Br angle (171.29(15)°), which lengthens the Ni-Br1B distance (2.419(3) Å) because of the stronger trans-influence of the alkyl ligand.

X-band EPR spectroscopic data of [Ni-CH]\* were collected in a 2-MeTHF glass at 77 K (Figure 3). Spectral

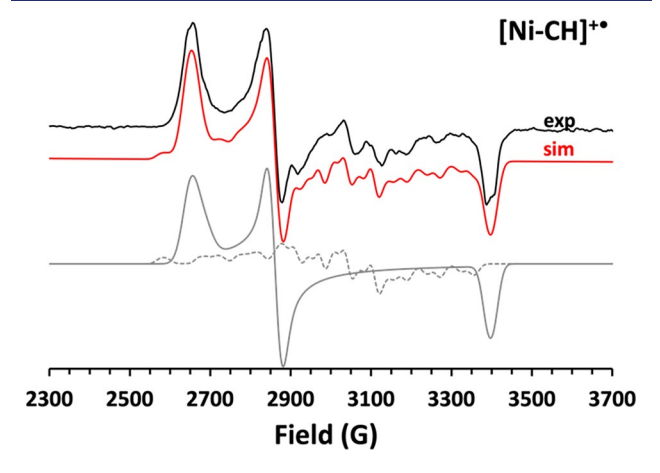


Figure 3. Top: Experimental (black) and simulated (red, offset) X-band EPR spectra of [Ni–CH]\*\* (77 K, 2-MeTHF glass). Bottom: Overlayed simulations of major spin component (solid gray line) and minor spin component (dashed gray line).

data were modeled as a two-component S=1/2 spin system with a 0.75:0.25 ratio of spin concentrations (red), consistent with the bromide positional disorder ratios observed at 100 K by X-ray crystallography (vide supra). The major spin component is modeled as a rhombic signal with g=1.9844, 2.3564, 2.5425 and isotropic hyperfine interactions assigned to two inequivalent P nuclei and one Br nucleus  $(a_{\rm iso}(^{31}{\rm P}_1)=\pm 19~{\rm MHz},~a_{\rm iso}(^{31}{\rm P}_2)=\pm 49~{\rm MHz},~a_{\rm iso}({\rm Br})=\pm 1~{\rm MHz};$  solid gray line). The minor component is also modeled as a rhombic signal (g=2.0931,~2.2461,~2.4091) but with anisotropic hyperfine interactions  $(A(^{31}{\rm P}_1)=\pm [30,15,61]~{\rm MHz},~A(^{31}{\rm P}_2)=\pm [90,~80,~456]~{\rm MHz},~A({\rm Br})=\pm [230,194,~317]~{\rm MHz};$  dashed gray line).

After full characterization of these Ni complexes, we sought to obtain the acidity of the agostic  $C(sp^3)-H-Ni$  interaction in THF. Complexes [Ni-CH],  $[Ni-CH_2]^+$ , and  $[Ni-CH]^{\bullet+}$  are interrelated through the ability of  $[Ni-CH_2]^+$  to release  $H^+$  or  $H^{\bullet}$  as shown in eqs 1 and 2. By extension, eq 3 describes the standard-state free energy relationships between these

equilibria, which also include the standard state Ni<sup>III/II</sup> reduction potential in THF (vide supra) and  $C_{\rm G,THF}$  (60.4  $\pm$  2 kcal mol<sup>-1</sup>).<sup>23</sup>

$$[\mathbf{Ni-CH_2}]^+ \rightleftharpoons [\mathbf{Ni-CH}] + \mathbf{H}^+ \quad \Delta G^\circ = 1.364 \text{ pK}_a^{\text{solv}}$$
(1)

$$[\mathbf{Ni} - \mathbf{CH}_2]^+ \rightleftharpoons [\mathbf{Ni} - \mathbf{CH}]^{\bullet +} + \mathbf{H}^{\bullet}$$

$$\Delta G^{\circ} = \mathbf{BDFE}_{\text{solv}}(\mathbf{C} - \mathbf{H})$$
(2)

BDFE<sub>THF</sub>(C—H) = 
$$1.364 \text{ pK}_{a}^{\text{THF}} + 23.06E^{\circ} + C_{G,\text{THF}}$$
(3)

Unfortunately,  $[\mathrm{Ni-CH_2}]^+$  is unstable in THF and MeCN, prompting us to use 1,2-dichloroethane (DCE) for all acidbase reactions. A collection of  $pK_{\mathrm{ip}}^{\mathrm{DCE}}$  values (ip = ion pair) for cationic acids have been measured in DCE and can be correlated with  $pK_{\mathrm{a}}^{\mathrm{MeCN}}$  values using eq 4.24 To transpose these acidities from MeCN to  $pK_{\mathrm{a}}^{\mathrm{THF},25}$  eq 5 has been developed for a large collection of cationic acids.26

$$pK_{ip}^{DCE} = pK_a^{MeCN} \times (0.99) - 3.93$$
 (4)

$$pK_a^{THF} = pK_aMeCN \times (0.98 \pm 0.02) - (6.1 \pm 0.4) + (0.84 \pm 0.16) \times 2$$
 (5)

Thus, [Ni-CH2]+ was reacted with bases of varying strengths and [Ni-CH2]+ was found to be compatible with para-substituted anilines in DCE. Equilibrium data were monitored via <sup>31</sup>P NMR spectroscopy. The reaction between [Ni-CH<sub>2</sub>]<sup>+</sup> and 2,6-dichloroaniline resulted in no deprotonation after 6 days (Figure S11). Mixing [Ni-CH<sub>2</sub>]<sup>+</sup> with the stronger base 4-methoxyaniline resulted in full deprotonation after 2 days to exclusively generate [Ni-CH] in solution. Using eq 4 and the known  $pK_a^{\text{MeCN}}$  values for the conjugate anilinium acids, the  $pK_{ip}^{\text{DCE}}$  of  $[\mathbf{Ni-CH_2}]^+$  lies between 1.1  $\pm$ 0.5 and 7.8  $\pm$  0.5. <sup>27</sup> Gratifyingly, addition of the intermediatestrength base 2,4-difluoroaniline (p $K_{\rm ip}^{\rm DCE}$  = 4.4 ± 0.5) yielded a mixture of [Ni–CH<sub>2</sub>]<sup>+</sup> and [Ni–CH] which reached equilibrium after ca. 11 days ( $K_{eq} = 0.35$ , Figure S12). Protonation of [Ni-CH] with [2,4-difluoroanilinium][B- $(C_6F_5)_4$  (i.e., the reverse reaction) produced a nearly identical product distribution, reaching equilibrium in about 4 h ( $K_{\rm eq}$  = 0.45, Figure S13). Using these data, the p $K_{\rm ip}^{\rm DCE}$  of [Ni–CH<sub>2</sub>]<sup>+</sup> is 4.8  $\pm$  0.5, resulting in p $K_{\rm a}^{\rm MeCN}$  = 8.8  $\pm$  0.5 and p $K_{\rm a}^{\rm THF}$  = 4.2  $\pm$  0.7 by using eqs 4 and 5 (Scheme 2, top). Previous estimates show that adamantane is an extremely weak acid  $(pK_a^{DMSO} \cong$ 54), 28 suggesting that the C-H bond is acidified by dozens of orders of magnitude upon coordination of PCH2P to the hypothetical [Ni<sup>II</sup>Br]<sup>+</sup> ion.<sup>29</sup>

Because of the incompatibility of [Ni-CH<sub>2</sub>]<sup>+</sup> and [Ni-CH]<sup>•+</sup> with several common PCET reagents, direct BDFE measurements could not be obtained. However, using eq 3, the BDFE<sub>THF</sub>(C-H) of [Ni-CH<sub>2</sub>]<sup>+</sup> is calculated to be 70 ± 2 kcal mol<sup>-1</sup>, giving a complete thermochemical cycle involving [Ni-CH]<sup>•+</sup>, [Ni-CH<sub>2</sub>]<sup>+</sup>, and [Ni-CH] (Scheme 2, bottom). For comparison, the C-H bond dissociation enthalpy (BDE) of 2-adamantane is 100 ± 3 kcal/mol,<sup>30</sup> indicating that solvation and coordination of free ligand PCH<sub>2</sub>P to [Ni<sup>II</sup>Br]<sup>+</sup> weakens the methylene C-H bonds of adamantane by around 30 kcal/mol (neglecting entropic contributions). To complement these thermochemical data, dispersion-corrected DFT calculations using isodesmic reaction schemes were used to independently

Scheme 2. Equilibrium Measurements in DCE (top) and Thermochemical Measurements in THF (bottom)<sup>a,b</sup>

[Ni-CH<sub>2</sub>]<sup>+</sup> + 
$$\bigvee_{F}^{NH_2}$$
 F  $\bigvee_{C=0}^{NH_2}$  [Ni-CH] +  $\bigvee_{F}^{NH_3^+}$  F  $\bigvee_{C=0}^{NH_3^+}$  P  $\bigvee_{C=0}^{NH_$ 

<sup>a</sup>The B(C<sub>6</sub>F<sub>5</sub>)<sub>4</sub><sup>-</sup> counterion is not shown. <sup>b</sup>Numbers in parentheses are calculated using DFT and the BDFE<sup>THF</sup> value in bold is calculated from the experimental  $E^{\circ}$  and p $K_4$  measurements.

determine p $K_a^{\rm THF}$  (3.7), BDFE (69.8 kcal/mol), and  $E^{\circ}$  (0.050 V) (Figure S21).<sup>31</sup> A multilevel approach was used where the DFT-optimized structures at a lower level of theory (TPSS-D3(BJ)/def2-TZVP) were used in single point energy calculations with the larger def2-QZVPP basis set<sup>18b,c</sup> and the PW6B95-D3(BJ) functional (see SI).<sup>32</sup> This functional was chosen for its good performance in the GMTKN55,<sup>33</sup> MOR41,<sup>34</sup> and ROST61<sup>35</sup> benchmark databases (see the SI for full computational details). Gratifyingly, the thermochemical values shown are in excellent agreement with experiment.

In summary, we have presented the first measurements of  $C(sp^3)$ —H agostic bond strength under conditions relevant to synthetic chemists, providing a deeper understanding of the thermochemical driving forces behind nickel-mediated C—H activation reactions. Work is ongoing to study the influence of the X-type ligand in these pincer systems and correlate agostic C—H bond strength with ancillary ligand environment.

# ASSOCIATED CONTENT

# Supporting Information

The Supporting Information is available free of charge at https://pubs.acs.org/doi/10.1021/jacs.2c05667.

DFT-Computed Cartesian coordinates (XYZ) Experimental details, spectra, voltammograms, selected crystallographic data, isodesmic reaction schemes (PDF)

#### **Accession Codes**

CCDC 2102261,2102262 and 2167539 contain the supplementary crystallographic data for this paper. These data can be obtained free of charge via www.ccdc.cam.ac.uk/data\_request/cif, or by emailing data\_request@ccdc.cam.ac.uk, or by contacting The Cambridge Crystallographic Data Centre, 12 Union Road, Cambridge CB2 1EZ, UK; fax: +44 1223 336033.

#### AUTHOR INFORMATION

## **Corresponding Author**

**Demyan E. Prokopchuk** – Department of Chemistry, Rutgers University-Newark, Newark, New Jersey 07102, United States; o orcid.org/0000-0002-6352-3509; Email: demyan.prokopchuk@rutgers.edu

#### **Authors**

Lirong Lin — Department of Chemistry, Rutgers University-Newark, Newark, New Jersey 07102, United States

Denis M. Spasyuk — Canadian Light Source, Saskatoon,
Saskatchewan S7N2V3, Canada; orcid.org/0000-0001-9018-3063

Roger A. Lalancette – Department of Chemistry, Rutgers University-Newark, Newark, New Jersey 07102, United States; orcid.org/0000-0002-3470-532X

Complete contact information is available at: https://pubs.acs.org/10.1021/jacs.2c05667

#### Notes

The authors declare no competing financial interest.

## ACKNOWLEDGMENTS

This research was supported by a Rutgers University—Newark startup grant. Single-crystal X-ray diffraction data were partly supported by the National Science Foundation under Grant 2018753. D.E.P. thanks the Office of Advanced Research Computing (OARC) at Rutgers for providing access to the Amarel cluster and Hagen Neugebauer (University of Bonn) for constructive DFT comments. D.E.P and L.L. thank Prof. Donald Hirsch (The College of New Jersey) for EPR assistance and Dr. Pavel Kucheryavy (Rutgers-Newark) for NMR assistance.

#### REFERENCES

- (1) (a) Tasker, S. Z.; Standley, E. A.; Jamison, T. F. Recent advances in homogeneous nickel catalysis. *Nature* **2014**, *509*, 299–309. (b) Xue, X.-S.; Ji, P.; Zhou, B.; Cheng, J.-P. The Essential Role of Bond Energetics in C–H Activation/Functionalization. *Chem. Rev.* **2017**, *117*, 8622–8648. (c) Campeau, L.-C.; Hazari, N. Cross-Coupling and Related Reactions: Connecting Past Success to the Development of New Reactions for the Future. *Organometallics* **2019**, 38, 3–35. (d) Gandeepan, P.; Müller, T.; Zell, D.; Cera, G.; Warratz, S.; Ackermann, L. 3d Transition Metals for C–H Activation. *Chem. Rev.* **2019**, *119*, 2192–2452.
- (2) Brookhart, M.; Green, M. L. H.; Parkin, G. Agostic interactions in transition metal compounds. *Proc. Natl. Acad. Sci. U.S.A.* **2007**, *104*, 6908–6914.
- (3) (a) Aihara, Y.; Chatani, N. Nickel-Catalyzed Direct Arylation of C(sp<sup>3</sup>)-H Bonds in Aliphatic Amides via Bidentate-Chelation Assistance. J. Am. Chem. Soc. 2014, 136, 898-901. (b) Wu, X.; Zhao, Y.; Ge, H. Nickel-Catalyzed Site-Selective Alkylation of Unactivated C(sp3)-H Bonds. J. Am. Chem. Soc. 2014, 136, 1789-1792. (c) Yang, Y.-F.; Chen, G.; Hong, X.; Yu, J.-Q.; Houk, K. N. The Origins of Dramatic Differences in Five-Membered vs Six-Membered Chelation of Pd(II) on Efficiency of C(sp<sup>3</sup>)-H Bond Activation. J. Am. Chem. Soc. 2017, 139, 8514-8521. (d) Davies, D. L.; Macgregor, S. A.; McMullin, C. L. Computational Studies of Carboxylate-Assisted C-H Activation and Functionalization at Group 8-10 Transition Metal Centers. Chem. Rev. 2017, 117, 8649-8709. (e) Beattie, D. D.; Grunwald, A. C.; Perse, T.; Schafer, L. L.; Love, J. A. Understanding Ni(II)-Mediated C(sp<sup>3</sup>)-H Activation: Tertiary Ureas as Model Substrates. J. Am. Chem. Soc. 2018, 140, 12602-12610. (f) Liu, J.; Johnson, S. A. Mechanism of 8-Aminoquinoline-Directed Ni-Catalyzed C(sp<sup>3</sup>)-H Functionalization: Paramagnetic Ni(II) Species and the Deleterious Effect of Carbonate as a Base. Organometallics **2021**, 40, 2970-2982.
- (4) (a) Lafrance, M.; Rowley, C. N.; Woo, T. K.; Fagnou, K. Catalytic Intermolecular Direct Arylation of Perfluorobenzenes. *J. Am. Chem. Soc.* **2006**, *128*, 8754–8756. (b) Gorelsky, S. I.; Lapointe, D.;

- Fagnou, K. Analysis of the Concerted Metalation-Deprotonation Mechanism in Palladium-Catalyzed Direct Arylation Across a Broad Range of Aromatic Substrates. *J. Am. Chem. Soc.* **2008**, *130*, 10848–10849. (c) Balcells, D.; Clot, E.; Eisenstein, O. C–H Bond Activation in Transition Metal Species from a Computational Perspective. *Chem. Rev.* **2010**, *110*, 749–823. (d) Christman, W. E.; Morrow, T. J.; Arulsamy, N.; Hulley, E. B. Absolute Estimates of  $Pd^{II}(\eta^2$ -Arene) C–H Acidity. *Organometallics* **2018**, *37*, 2706–2715. (e) Carrow, B. P.; Sampson, J.; Wang, L. Base-Assisted C–H Bond Cleavage in Cross-Coupling: Recent Insights into Mechanism, Speciation, and Cooperativity. *Isr. J. Chem.* **2020**, *60*, 230–258.
- (5) Christman, W. E.; Morrow, T. J.; Arulsamy, N.; Hulley, E. B. Absolute Estimates of PdII( $\eta$ 2-Arene) C-H Acidity. *Organometallics* **2018**, *37*, 2706–2715.
- (6) Vigalok, A.; Uzan, O.; Shimon, L. J. W.; Ben-David, Y.; Martin, J. M. L.; Milstein, D. Formation of  $\eta^2$  C–H Agostic Rhodium Arene Complexes and Their Relevance to Electrophilic Bond Activation. *J. Am. Chem. Soc.* **1998**, *120*, 12539–12544.
- (7) Murugesan, S.; Stöger, B.; Pittenauer, E.; Allmaier, G.; Veiros, L. F.; Kirchner, K. A Cobalt(I) Pincer Complex with an  $\eta^2$ -Caryl—H Agostic Bond: Facile C—H Bond Cleavage through Deprotonation, Radical Abstraction, and Oxidative Addition. *Angew. Chem., Int. Ed.* **2016**, *55*, 3045–3048.
- (8) (a) Gusev, D. G.; Lough, A. J. Double C–H Activation on Osmium and Ruthenium Centers: Carbene vs Olefin Products. Organometallics **2002**, 21, 2601–2603. (b) Kuznetsov, V. F.; Abdur-Rashid, K.; Lough, A. J.; Gusev, D. G. Carbene vs Olefin Products of C–H Activation on Ruthenium via Competing  $\alpha$  and  $\beta$ -H Elimination. J. Am. Chem. Soc. **2006**, 128, 14388–14396. (c) Burford, R. J.; Piers, W. E.; Parvez, M.  $\beta$ -Elimination-Immune PC<sub>carbene</sub>P Iridium Complexes via Double C–H Activation: Ligand-Metal Cooperation in Hydrogen Activation. Organometallics **2012**, 31, 2949–2952.
- (9) Gerber, R.; Blacque, O.; Frech, C. M. Suzuki Cross-Coupling Reactions Catalyzed by an Aliphatic Phosphine-Based Pincer Complex of Palladium: Evidence for a Molecular Mechanism. *ChemCatChem.* **2009**, *1*, 393–400.
- (10) Averina, E. B.; Sedenkova, K. N.; Bakhtin, S. G.; Grishin, Y. K.; Kutateladze, A. G.; Roznyatovsky, V. A.; Rybakov, V. B.; Butov, G. M.; Kuznetsova, T. S.; Zefirov, N. S. symm-Tetramethylenecyclooctane: En Route to Polyspirocycles. *J. Org. Chem.* **2014**, *79*, 8163–8170.
- (11) (a) Fine, D. A. Tetrahedral Bromide Complexes of Nickel(II) in Organic Solvents. *Inorg. Chem.* **1965**, *4*, 345–350. (b) Alyea, E. C.; Costin, A.; Ferguson, G.; Fey, G. T.; Goel, R. G.; Restivo, R. J. Synthesis, crystal, and molecular structure of paramagnetic tri-t-butylphosphonium tribromo(tri-t-butylphosphine)nickelate(II). *J. Chem. Soc., Dalton Trans.* **1975**, 1294–1298.
- (12) Castonguay, A.; Sui-Seng, C.; Zargarian, D.; Beauchamp, A. L. Syntheses and Reactivities of New PCsp<sup>3</sup>P Pincer Complexes of Nickel. *Organometallics* **2006**, 25, 602–608.
- (13) (a) Rach, S. F.; Herdtweck, E.; Kühn, F. E. A straightforward synthesis of cationic nitrile ligated transition metal complexes with the  $[B(C_6F_5)_4]^-$  anion. *J. Organomet. Chem.* **2011**, 696, 1817–1823. (b) Heiden, Z. M.; Chen, S.; Mock, M. T.; Dougherty, W. G.; Kassel, W. S.; Rousseau, R.; Bullock, R. M. Protonation of Ferrous Dinitrogen Complexes Containing a Diphosphine Ligand with a Pendent Amine. *Inorg. Chem.* **2013**, 52, 4026–4039. (c) Jutzi, P.; Müller, C.; Stammler, A.; Stammler, H.-G. Synthesis, Crystal Structure, and Application of the Oxonium Acid  $[H(OEt_2)_2]^+[B(C_6F_5)_4]^-$ . *Organometallics* **2000**, 19, 1442–1444.
- (14) (a) Marks, T. J.; Kolb, J. R. Covalent transition metal, lanthanide, and actinide tetrahydroborate complexes. *Chem. Rev.* 1977, 77, 263–293. (b) Xu, Z.; Lin, Z. Transition metal tetrahydroborato complexes: an orbital interaction analysis of their structure and bonding. *Coord. Chem. Rev.* 1996, 156, 139–162.
- (15) (a) Baratta, W.; Mealli, C.; Herdtweck, E.; Ienco, A.; Mason, S. A.; Rigo, P. Nonclassical vs Classical Metal····H<sub>3</sub>C-C Interactions: Accurate Characterization of a 14-Electron Ruthenium(II) System by

- Neutron Diffraction, Database Analysis, Solution Dynamics, and DFT Studies. *J. Am. Chem. Soc.* **2004**, *126*, 5549–5562. (b) Crosby, S. H.; Clarkson, G. J.; Rourke, J. P. A Delicate Balance between sp<sup>2</sup> and sp<sup>3</sup> C–H Bond Activation: A Pt(II) Complex with a Dual Agostic Interaction. *J. Am. Chem. Soc.* **2009**, *131*, 14142–14143.
- (16) Beattie, D. D.; Bowes, E. G.; Drover, M. W.; Love, J. A.; Schafer, L. L. Oxidation State Dependent Coordination Modes: Accessing an Amidate-Supported Nickel(I)  $\delta$ -bis(C-H) Agostic Complex. *Angew. Chem., Int. Ed.* **2016**, *55*, 13290–13295.
- (17) He, W.; Beattie, D. D.; Zhou, H.; Bowes, E. G.; Schafer, L. L.; Love, J. A.; Kennepohl, P. Direct metal—carbon bonding in symmetric bis(C-H) agostic nickel(i) complexes. *Chem. Sci.* **2021**, *12*, 15298—15307.
- (18) (a) Tao, J.; Perdew, J. P.; Staroverov, V. N.; Scuseria, G. E. Climbing the Density Functional Ladder: Nonempirical Meta-Generalized Gradient Approximation Designed for Molecules and Solids. *Phys. Rev. Lett.* **2003**, *91*, 146401. (b) Weigend, F.; Ahlrichs, R. Balanced basis sets of split valence, triple zeta valence and quadruple zeta valence quality for H to Rn: Design and assessment of accuracy. *Phys. Chem. Chem. Phys.* **2005**, *7*, 3297–3305. (c) Weigend, F. Accurate Coulomb-fitting basis sets for H to Rn. *Phys. Chem. Chem. Phys.* **2006**, *8*, 1057–1065.
- (19) (a) Lu, Q.; Neese, F.; Bistoni, G. Formation of Agostic Structures Driven by London Dispersion. *Angew. Chem., Int. Ed.* **2018**, *57*, 4760–4764. (b) Grimme, S.; Antony, J.; Ehrlich, S.; Krieg, H. A consistent and accurate ab initio parametrization of density functional dispersion correction (DFT-D) for the 94 elements H-Pu. *J. Chem. Phys.* **2010**, *132*, 154104. (c) Grimme, S.; Ehrlich, S.; Goerigk, L. Effect of the damping function in dispersion corrected density functional theory. *J. Comput. Chem.* **2011**, *32*, 1456–1465.
- (20) LeSuer, R. J.; Geiger, W. E. Improved Electrochemistry in Low-Polarity Media Using Tetrakis(pentafluorophenyl)borate Salts as Supporting Electrolytes. *Angew. Chem., Int. Ed.* **2000**, *39*, 248–250.
- (21) O'Connor, A. R.; Nataro, C.; Golen, J. A.; Rheingold, A. L. Synthesis and reactivity of  $[N(C_6H_4Br)_3][B(C_6F_5)_4]$ : the X-ray crystal structure of  $[Fe(C_5H_5)_2][B(C_6F_5)_4]$ . J. Organomet. Chem. **2004**, 689, 2411–2414.
- (22) Yang, L.; Powell, D. R.; Houser, R. P. Structural variation in copper(i) complexes with pyridylmethylamide ligands: structural analysis with a new four-coordinate geometry index, [small tau]4. *Dalton Trans.* **2007**, 955–964.
- (23) Wise, C. F.; Agarwal, R. G.; Mayer, J. M. Determining Proton-Coupled Standard Potentials and X–H Bond Dissociation Free Energies in Nonaqueous Solvents Using Open-Circuit Potential Measurements. *J. Am. Chem. Soc.* **2020**, *142*, 10681–10691.
- (24) Kaupmees, K.; Järviste, R.; Leito, I. Basicity of Very Weak Bases in 1,2-Dichloroethane. *Chem. Eur. J.* **2016**, *22*, 17445–17449.
- (25) More specifically, this  $pK_a$  value is a  $pK_a$  measurement, which is an estimated  $pK_a$  based on the directly measured ion-pair acidity that is corrected using the Fuoss equation. For more information, see: Abdur-Rashid, K.; Fong, T. P.; Greaves, B.; Gusev, D. G.; Hinman, J. G.; Landau, S. E.; Lough, A. J.; Morris, R. H. An Acidity Scale for Phosphorus-Containing Compounds Including Metal Hydrides and Dihydrogen Complexes in THF: Toward the Unification of Acidity Scales. *J. Am. Chem. Soc.* **2000**, *122*, 9155.
- (26) Tshepelevitsh, S.; Kütt, A.; Lõkov, M.; Kaljurand, I.; Saame, J.; Heering, A.; Plieger, P. G.; Vianello, R.; Leito, I. On the Basicity of Organic Bases in Different Media. *Eur. J. Org. Chem.* **2019**, 2019, 6735–6748.
- (27) Kütt, A.; Tshepelevitsh, S.; Saame, J.; Lõkov, M.; Kaljurand, I.; Selberg, S.; Leito, I. Strengths of Acids in Acetonitrile. *Eur. J. Org. Chem.* **2021**, 2021, 1407–1419.
- (28) Kruppa, G. H.; Beauchamp, J. L. Energetics and structure of the 1- and 2-adamantyl radicals and their corresponding carbonium ions by photoelectron spectroscopy. *J. Am. Chem. Soc.* **1986**, *108*, 2162–2169.
- (29) We stress that great caution must be taken when directly comparing  $pK_a$  data in different organic media.

- (30) Aubry, C.; Holmes, J. L.; Walton, J. C. 1- and 2-Adamantyl Radicals and Cations in the Gas Phase: Thermochemistry and Mass Spectrometry. *J. Phys. Chem. A* **1998**, *102*, 1389–1393.
- (31) (a) Chen, S.; Rousseau, R.; Raugei, S.; Dupuis, M.; DuBois, D. L.; Bullock, R. M. Comprehensive Thermodynamics of Nickel Hydride Bis(Diphosphine) Complexes: A Predictive Model through Computations. *Organometallics* **2011**, *30*, 6108–6118. (b) Chen, S.; Ho, M.-H.; Bullock, R. M.; DuBois, D. L.; Dupuis, M.; Rousseau, R.; Raugei, S. Computing Free Energy Landscapes: Application to Nibased Electrocatalysts with Pendant Amines for H<sub>2</sub> Production and Oxidation. *ACS Catal.* **2014**, *4*, 229–242. (c) Raugei, S.; DuBois, D. L.; Rousseau, R.; Chen, S.; Ho, M.-H.; Bullock, R. M.; Dupuis, M. Toward Molecular Catalysts by Computer. *Acc. Chem. Res.* **2015**, *48*, 248–255. (d) Kuo, J. L.; Gunasekara, T.; Hansen, A.; Vibbert, H. B.; Bohle, F.; Norton, J. R.; Grimme, S.; Quinlivan, P. J. Thermodynamics of H<sup>+</sup>/H<sup>•</sup>/H<sup>-</sup>/e<sup>-</sup> Transfer from [CpV(CO)<sub>3</sub>H]<sup>-</sup>: Comparisons to the Isoelectronic CpCr(CO)<sub>3</sub>H. *Organometallics* **2019**, *38*, 4319–4328.
- (32) Zhao, Y.; Truhlar, D. G. Design of Density Functionals That Are Broadly Accurate for Thermochemistry, Thermochemical Kinetics, and Nonbonded Interactions. *J. Phys. Chem. A* **2005**, *109*, 5656–5667.
- (33) Goerigk, L.; Hansen, A.; Bauer, C.; Ehrlich, S.; Najibi, A.; Grimme, S. A look at the density functional theory zoo with the advanced GMTKN55 database for general main group thermochemistry, kinetics and noncovalent interactions. *Phys. Chem. Chem. Phys.* **2017**, *19*, 32184–32215.
- (34) Dohm, S.; Hansen, A.; Steinmetz, M.; Grimme, S.; Checinski, M. P. Comprehensive Thermochemical Benchmark Set of Realistic Closed-Shell Metal Organic Reactions. *J. Chem. Theory Comput.* **2018**, 14, 2596–2608.
- (35) Maurer, L. R.; Bursch, M.; Grimme, S.; Hansen, A. Assessing Density Functional Theory for Chemically Relevant Open-Shell Transition Metal Reactions. *J. Chem. Theory Comput.* **2021**, *17*, 6134–6151.